# Fractal nature of viscous fingering in three-dimensional pore-level models

M. Ferer and Jared C. Gump
*Department of Physics, West Virginia University, P.O. Box 6315, Morgantown, West Virginia 26506-6315*

Duane H. Smith
*U.S. Department of Energy, Morgantown Energy Technology Center, Morgantown, West Virginia 26507-0880*
(Received 27 September 1995)

Using three-dimensional pore-level models of random porous media, we have studied viscous fingering in "two-phase," miscible flow. When the viscosity ratio $M$ ($= \mu_D/\mu_I$), the ratio of the viscosity of the displaced fluid to that of the injected fluid, is infinite, the flow is known to be modeled by diffusion-limited aggregation (DLA). We have observed and characterized the crossover from fractal flow at short times or large viscosity ratios to compact (i.e., Euclidean) flow at later times. In our pore-level model of three-dimensional flow in the limit of infinite capillary number (zero surface tension), the low viscosity fluid is injected at constant pressure on one face of the model porous medium. This modeling shows that this flow is fractal for large viscosity ratios ($M = 10\,000$), consistent with DLA. For realistic viscosities ($M$=30–1000), our modeling of the unstable flow shows that, although the flows are initially fractal, they become linear on a time scale $\tau$, increasing as $\tau = \tau_0 M^{0.16}$. This characteristic crossover time predicts that the flow become compact for patterns larger than a characteristic length, which increases with viscosity ratio as $l = l_0 M^{0.16/(D_f-2)}$, where $D_f$ is the fractal dimension. Once compact, the saturation front advances as $x \approx v_0 M^{0.16} t$; the factor $M^{0.16}$ acts as a three-dimensional Koval factor.

PACS number(s): 68.10.−m, 47.55.Mh, 03.40.Gc

## I. INTRODUCTION

Nonequilibrium fractal growth has been observed in a wide variety of two- and three-dimensional (2D and 3D) Laplacian systems [1–3], from fluid flow in porous media with the characteristic viscous fingering [4–6] to fracturing [7] to electrochemical deposition [8–10] to fractal river networks [11,12] to dielectric breakdown [13] etc. The relaxation of such systems from nonequilibrium, fractal growth to Euclidean or compact growth has also been observed for two-phase flow in porous media [4–6] and for electrochemical deposition [14,15]. Much of this work has focused on the more easily visualized two-dimensional systems, but some have observed the crossover or relaxation in three-dimensional systems [5,15].

In a series of earlier papers [16–19], we studied two-phase flow in 2D Porous media as the flow crossed over (or relaxed) from fractal flow at infinite viscosity ratio ($M = \mu_D/\mu_I$; the injected fluid has zero viscosity) to compact flow at finite viscosity ratio. In these papers, we have characterized various aspects of the two-phase flow as it relaxed from nonequilibrium, fractal advance at the shorter times or the larger viscosity ratios to equilibrium, compact flow at the longer times or smaller viscosity ratios. We determined the "crossover," or relaxation, time $\tau \approx M^{0.17}$ (or the corresponding crossover length $l \approx \tau^{1/(D_f-1)}$) characterizing the time scale on which this crossover occurs for both radial [16] and linear [17] interfacial advance as well as for the roughness of the interface [18]. In addition to characterizing the relaxation time scale, incorporation of this relaxation time in a "fractal" scaling description of density and current profiles leads to a determination of the viscosity-ratio dependence of composition dependent relative mobilities [19], which are used in all traditional modeling of flow in porous media, such as Buckley-Leverett, Koval, etc. [20,21].

In this paper, we extend our 2D determination of the relaxation time to three dimensions. Before presenting details of our work, we briefly review salient features of (i) DLA fractals in 3D, (ii) viscous fingering, (iii) aspect ratio concerns, and (iv) characteristic density and fractional flow.

The classic signature of a mass fractal is a non-Euclidean relationship between mass and size. If one has an ordinary compact sphere, the mass is proportional to $R^3$, but for a spherical fractal object the mass is proportional to $R^{D_f}$, with a noninteger fractal dimension $D_f$; e.g., for DLA, $D_f \approx 2.5$ [22,23]. Therefore, a fractal object is less dense than an ordinary object because of material voids inside the object. However, it should be emphasized that neither the mass density nor the compensating voids are uniformly distributed; indeed, the mass density decreases with $R$, while the void density must increase with $R$.

Formation of these fractals is an unstable, nonequilibrium process [2,3,24]. For "unstable" flow (i.e., viscosity ratio $M > 1$), the injected fluid fingers into the displaced fluid [25]. This effect has been widely studied in 2D "Hele-Shaw" cells, where a high viscosity fluid occupies the space between two closely spaced glass plates, and a low viscosity fluid is injected at the center. If the velocity ratio is large enough, the viscous-fingering patterns satisfy a fractal relationship $m \approx R^{D_f}$, with 2D fractal dimension $D_f = 1.70 \pm 0.05$ [1]. If the space between the Hele-Shaw plates is filled with a bead pack, forming a ran-

 

dom porous medium, analysis of the fingering for large viscosity ratio (air into epoxy) produces a fractal with the essentially identical dimension of $D_f = 1.62 \pm 0.04$ [26]. Although we are unaware of similar determinations of fractal dimension from very-large-viscosity-ratio, 3D, viscous-fingering experiments, small-scale, 3D electrodeposits have shown DLA-like fractal behavior with a fractal dimension $D_f \approx 2.5$ [9,15].

In the analysis of fractal DLA patterns in 2D, it is known that large aspect ratios (long narrow systems) can give misleading results. In fractal growth, the patterns initially have many small fingers, some of which grow faster than others. The longer fingers grow more rapidly than the short fingers, so that as the object grows it "coarsens" (it has fewer and fewer growing fingers) [27]. Therefore, if the system is wide enough, at an advanced stage of growth the pattern has fingers on many different size scales, giving a nonuniform density (or saturation) profile. For DLA-like flow in a short-wide system, no single finger is dominant (Fig. 1) [27,28]; and the average position of the injected fluid $\langle x \rangle$ (related to the location of the front) has a nonlinear power-law dependence on the total saturation, or time $t$,

$$\langle x \rangle = Ct^{1+\varepsilon} , \tag{1}$$

where

$$1 + \varepsilon = 1/[D_f - (d-1)] .$$

For 3D, DLA-like flow has a fractal dimension $D_f \approx 2.5$, so that $\varepsilon \approx 1.0$ [22,23]. Therefore, we study systems that are no larger in the flow direction than in the other spatial directions to ensure that the relaxation to compact flow is not merely an artifact of the large aspect ratio of our systems. We then discuss our modeling of two-phase flow in three-dimensional porous media and present results that show that the flow is unambiguously fractal for a large viscosity ratio, $M = 10\,000$.

In modeling unstable, two-phase flow in porous media, we have used one of the most standard and most physically rigorous models possible. Variants of this model have been widely used to study various aspects of the flow in porous media [29–31]. This previous work verified that the flows were fractal for large viscosity ratios and that the flows were linear (or compact) for small viscosity ratios, which is consistent with our quantitative characterization of a crossover from small-scale fractal flow to large-scale linear (or compact) flows. For those readers not familiar with these models from previous work, a detailed discussion was presented in a previous publication [19]. Our studies used a standard cubic lattice model of homogeneous 3D porous media [4,29,32], in which the pore bodies, at the sites of the cubic lattice, all have unit volume but the cross-sectional area of each pore throat is randomly chosen from a uniform distribution, which is known to give random, fractal flow for infinite viscosity ratio in 2D [29]. To model flow in the limit of infinite capillary number, we use Poiseuille's law to determine the conductances (or transmissibilities) from the geometry and the location of the interface; we then use an extrapolated Gauss-Seidel iteration [19,33] of the discrete Laplace equation to determine the pressure field. Given the pressure drops across the throats and the conductances, Poiseuille's law enables us to determine the flow rate for each throat. We then use a straightforward deterministic procedure to advance the interface through a short time $\Delta t$. Flow is allowed in every throat; and the deterministic flow velocity is allowed to advance or retreat the interface within the pore throat, into its connecting pore body, and through a pore body into its outflow throats. Our simulations of flow for this model satisfy total fluid conservation to within 0.5%, even after

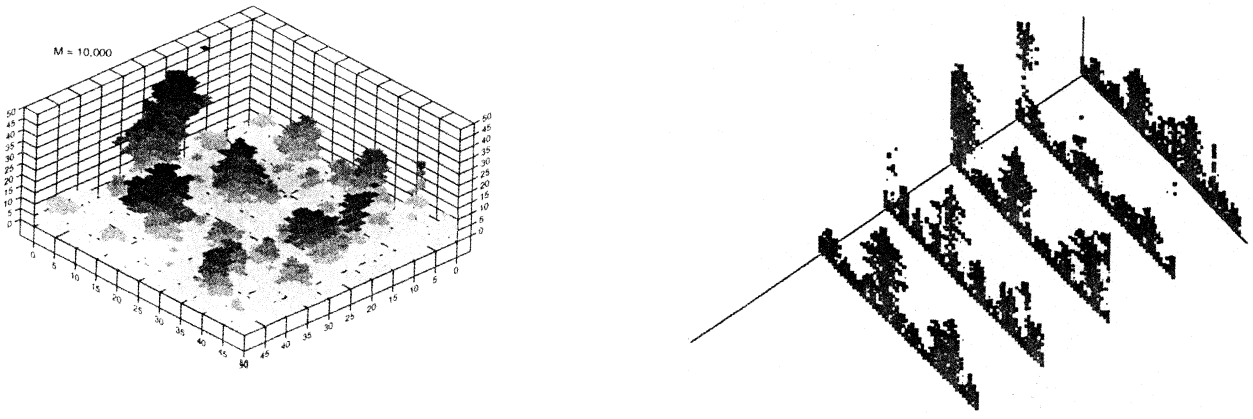


FIG. 1. Near-breakthrough flow pattern showing the pore bodies and throats occupied by injected fluid for a $50 \times 50 \times 50$ porous medium resulting from our simulations with a fluid velocity ratio $M = 10\,000$. For clarity, we present both a shaded 3D plot (on the left), in which the gray scale darkens with height, and projections of slices (on the right). The periodic boundary conditions are obvious in that fingers on one side continue on the other (notably, in the middle slice; also there is a connection between fingers ending in the last slice and starting in the first). The characteristics of DLA patterns are present: many short fingers coarsening to fewer and fewer longer fingers.

1400 time steps. This procedure has the advantage of not suppressing fractal flow [4], as do averaged methods like the grid-block procedures [34]; indeed, earlier variants of this model were used to study fractal flow [4,29,34].

In Sec. III, we address the question: Is viscous fingering fractal for realistic viscosity ratios? Using the model discussed above and detailed in [19], we study the time dependence of the first moment, i.e., $\langle x(t)\rangle$, for viscosity ratios $M = 30$ to 1000. For these viscosity ratios and probably for all finite viscosity ratios, the simulations produce initial fractal flows obeying Eq. (1), which become compact (or linear),

$$\langle x\rangle = vt \ , \tag{2}$$

on a characteristic time scale that increases with viscosity ratio. Our assumption of negligible dispersion should be a worst-possible-case scenario for fractal-to-compact crossover in the limit of infinite capillary number because dispersion will smooth the interface, thereby favoring compact flow and accelerating the fractal-to-compact crossover. Extending the "fractal" scaling [2,3,19,27] of saturation profile and fractional flow to include finite viscosity ratios enables us to determine a three-dimensional "Koval"-like factor in the post-crossover, compact-flow regime [35].

## II. FRACTAL VISCOUS FINGERING FOR LARGE VISCOSITY RATIOS

Next, we show that our modeling produces fractal flow for a large viscosity ratio, enabling us to check the predictions in Eq. (1). Using a viscosity ratio of 10 000, we ran our modeling program up to breakthrough for a number of different realizations of our model porous medium, all of which had a height $N_x$ and a square base (with $N \times N$ pore bodies); in each case, the height was no greater than the width of the base ($N_x \leq N$) to ensure that no one finger became dominant, giving pseudostable flow. Each of these realizations was generated by starting with a different seed for the random number generator on our floating point systems (FPS) machine. The five largest realizations were $N_x = 50$ pore bodies long in the flow direction and $50 \times 50$ perpendicular to the flow direction. Figure 1 shows a typical, near-breakthrough pattern for one of these $50 \times 50 \times 50$ porous media; this pattern does appear to be fractal, having fingers of many different sizes and looking very much like the patterns from on-lattice DLA simulations [3,27]. In addition to these five largest systems, we studied the flow in a number of realizations of different sizes [12 $30 \times 30 \times 30$ systems and six $(N_x = 30) \times 50 \times 50$ systems] in order to ensure that size effects were not affecting our analysis. We also ran three systems that were longer than they were wide [$(N_x = 50) \times 30 \times 30$]; for these systems, the onset of pseudostable flow due to the dominance of one viscous finger arose at later times, but it did not arise in any of the other systems we studied. In the $y$ and $z$ directions, we chose to use periodic boundary conditions in order to minimize edge and size effects.

During each of these runs, we have determined the time (mass of injected fluid) and $\langle x\rangle$ (average position of injected fluid along the flow direction) at each time step. To verify that our model with this large a viscosity ratio ($M = 10\,000$) is producing fractal flow, we have studied the dependence of $\langle x\rangle$ on $t$. Figure 2 shows the log-log plot of $\langle x\rangle/t^2$ vs $t$. Our specific definition of $t$ is proportional to the total volume of injected fluid $V_{\rm tot}$, which is also proportional to the total saturation, or total mass, through the relation

$$t = 1.34 + (V_{\rm tot}/N^2) \ . \tag{3}$$

For this linear flow problem, where low viscosity fluid is injected into all the $N \times N$ inlet pore bodies along the base, the factor of $N^2$ in Eq. (3) accounts for the areal dependence of the injection rate, allowing us to compare systems of different base area. The additive factor of $\{\Delta t = 1.34\}$ shifts the time origin; a similar value of $\{\Delta x = 0.672\}$ was added to $\langle x\rangle$ to shift the space origin. These values were determined by a least-squares fit of $\langle x\rangle + \Delta x = A(t+\Delta t)^2$ to these data. These shifts serve to remove early time curvature in Fig. 2; their effect at later times is insignificant. These shifts are similar in spirit to a shift in the location of $x = 0$, used in earlier DLA work to remove early time (short-distance) curvature [27], as well as to a shift in the time origin in our earlier 2D work [17]. If the flow is a DLA-like fractal, $\langle x\rangle/t^2$ will be constant for all $t$. The points track the results from runs on individual realizations of porous media. Finite-size effects seem negligible in the near-breakthrough data, since results for the smaller systems near breakthrough (near $t \approx 6$, the $N_x = 30$ models reach breakthrough) are statistically indistinguishable from results for the larger systems ($50 \times 50 \times 50$) well before breakthrough. The solid circles show the results of a data smoothing procedure in which we performed a quadratic least-squares fit of all the data [$y = \ln(\langle x\rangle/t)$, $x = \ln t$], with $x = \ln t$ in the interval $(\ln t_i - \frac{1}{4}, \ln t_i + \frac{1}{4})$; this gives the location of the $i$th solid

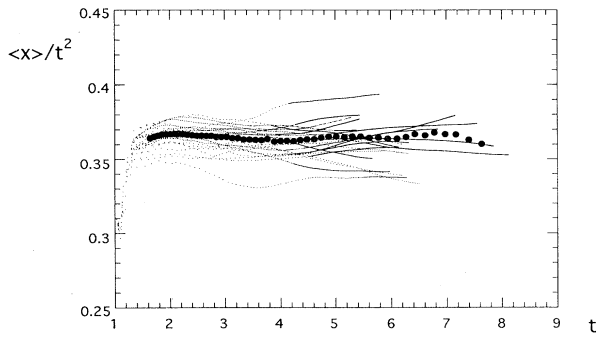


FIG. 2. Fractal behavior of the average position (i.e., $\langle x\rangle = Ct^2$) from modeling large viscosity-ratio flows with $M = 10\,000$ on different realizations of the porous medium. The dots track the flow for individual realizations, and the solid circles result from the data smoothing procedure.

circle $[(\langle x\rangle/t)_i, t_i]$ and its standard error. We then let $\ln t_i$ scan the full range of the data. The standard errors are no bigger than the solid circles used in Fig. 2. The first moment does, indeed, show fractal scaling ($\langle x\rangle \propto t^2$), which from Eq. (1) is consistent with the DLA value of the fractal dimension, $D_f = 2.53 \pm 0.06$ [22]. To estimate the effect of this uncertainty in the value of 2.5, we fit $\langle x\rangle + \Delta x = A(t + \Delta t)^{1+\epsilon}$ to the data for several values of $\epsilon$ in the range 0.70–1.0–1.63. It is clear that our data are not consistent with the more extreme values of the exponent, but these data do not obviously distinguish between $\epsilon$ in the range 0.90–1.4 (equivalently $D_f$ in the range 2.42–2.55).

To summarize, the flow is a DLA-like fractal for very large viscosity ratios. Furthermore, our data favor a value of fractal dimension nearer the "best value" of the DLA fractal dimension $D_f \approx 2.5$, rather than a value at the upper extremes of the allowed range, $D_f = 2.53 \pm 0.06$ [22].

## III. IS VISCOUS FINGERING FRACTAL FOR REALISTIC, UNSTABLE VISCOSITY RATIOS?

To study the nature of large-scale flows for finite viscosity ratio, we have modeled flows for realistic, unstable viscosity ratios: $M = 30$, 100, 300, and 1000. For each viscosity ratio, we have used a number of different realizations of our model porous medium to improve statistics. Figure 3 shows the near-breakthrough flow pattern for three viscosity ratios; this figure demonstrates the previously observed tendency of large viscosity-ratio flows to appear fractal while small viscosity-ratio flows are visibly more compact [4]. The fragmentation observed for the smaller viscosity ratios (e.g., $M = 30$) results from fluctuations in the pressure gradient perpendicular to average flow. Without capillary pressure, very small pressure gradients can produce flow; thus it is not surprising that fluctuations in the pressure field do produce a sign change in the small pressure gradient, producing back

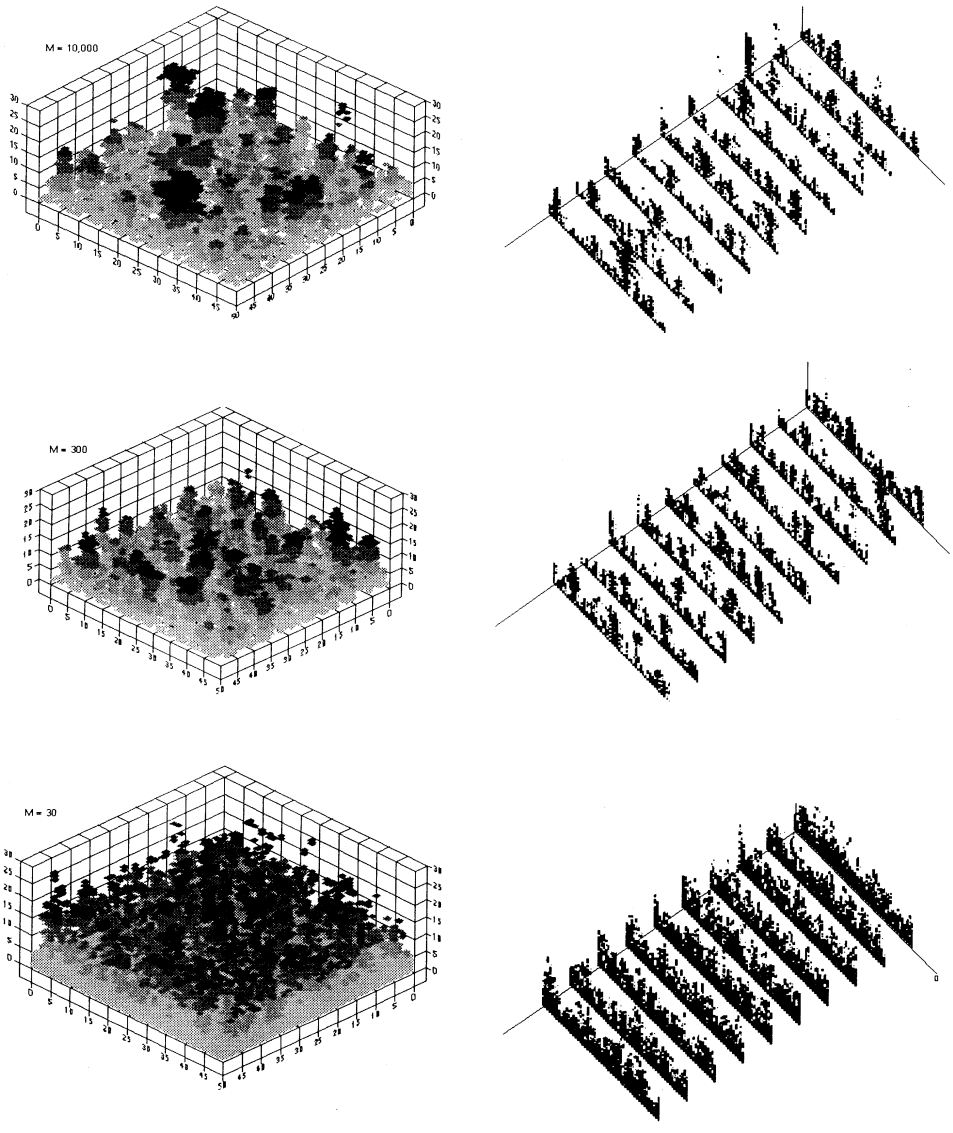


FIG. 3. Near-breakthrough flow patterns (both shaded 3D and projections of slices) show the locations of pore bodies occupied by injected fluid for three different viscosity ratios, $M = 10\,000$, 300, and 30. Note the apparent crossover from the fractal, DLA-like pattern at $M = 10\,000$ to compact flow with a rough interface at $M = 30$. Because of fluctuations in the pressure gradient perpendicular to the primary flow direction, we find the same fragmentation of the interface for $M = 30$, observed in 2D for linear flow with the smaller viscosity ratios.

flow that can pinch off fingers. This effect was nearly absent in 2D radial flow, where such fluctuations should be less significant [16]. To quantify the observed crossover from fractal flow to compact flow as a function of viscosity ratio and time, we have determined the average position of saturation $\langle x \rangle$ and the time $t$ [Eq. (3)] at each time step in the simulations. Performing these simulations for a number of different realizations of the model porous medium, we smoothed the resulting data, as described above, for each viscosity ratio. Figure 4 shows the smoothed data for $\langle x \rangle / t$ vs $t$ for all the viscosity ratios studied; as before, the standard errors are no larger than the data points. As expected from the above, the data for $M = 10\,000$ show fractal behavior with $\langle x \rangle / t$ growing as $t$. For the smaller viscosity ratios, the curves first follow the fractal $t$ dependence; but, beginning with the $M = 30$ data, they all break away from the fractal behavior and approach a constant, $\langle x \rangle / t = v$, characteristic of compact (linear) flow. Furthermore, this breakaway or crossover occurs on a characteristic time scale $\tau$, which increases with viscosity ratio. Figure 4 shows a well-defined crossover from initial fractal growth ($\langle x \rangle / t \approx t$) to eventual compact growth ($\langle x \rangle / t = -v$) for all relevant viscosity ratios.

To quantify this process, it is necessary to determine the viscosity ratio dependence of the front velocity $v(M)$ and characteristic crossover time $\tau(M)$. To determine a "scaling" variable [characteristic crossover time $\tau(M)$] that will collapse all the data onto a single curve, consider the data for $\langle x \rangle / t^2$, shown in Fig. 5. All the data start from a value 0.365, characteristic of the fractal dependence, and eventually cross over to the compact behavior with a $t^{-1}$ dependence. One can obtain a crude collapse of the data by plotting the data vs a "scaling" variable $t/M^{0.21}$, as shown in Fig. 6, where the characteristic time factor $M^{0.21}$ shifts the large viscosity-ratio data onto the smaller viscosity-ratio data. This estimate for the viscosity-ratio dependence of the relaxation time, i.e., $\tau \approx \tau_0 M^{0.21}$, appears to provide convincing data collapse for large times but not for the small-time regime near $t/M^{0.21} \approx 2$, where there still remains a small viscosity-ratio dependent spread in the data. Recalling that a shift $\Delta$ of the time origin was needed to obtain convincing fits in 2D [17], we found that including a small viscosity-ratio dependent time shift $\Delta = 2/M^{0.16}$ enabled us to obtain a somewhat more convincing data collapse with the "scaling" variable $u = \{t + (2/M^{0.16})\}/M^{0.16}$, as shown in Fig. 7. It should be noted that the index characterizing

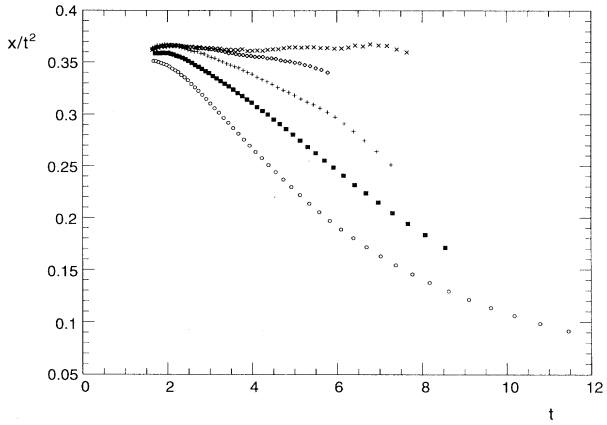


FIG. 5. Plot of $\langle x \rangle / t^2$ vs $t$ from the smoothed data for all viscosity ratios, showing the crossover from initial fractal behavior (constant) to eventual compact behavior ($t^{-1}$ dependence) on a characteristic time scale $\tau$, which increases with viscosity ratio. $M = 30$ (○), 100 (+), 300 (■), 1000 (◇), and 10 000 (×).

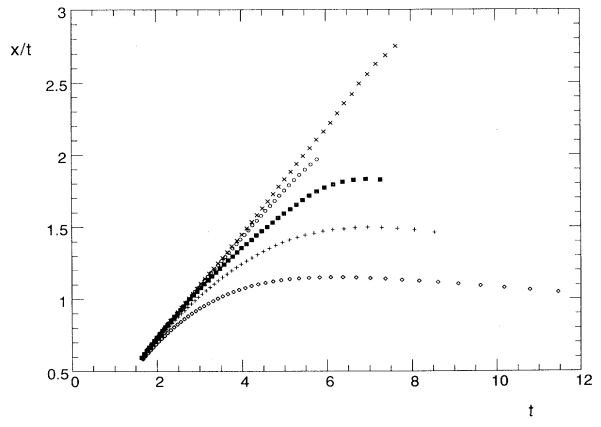


FIG. 4. Smoothed data for $\langle x \rangle / t$ vs $t$, showing the crossover from initial fractal growth ($t$ behavior) to eventual compact growth ($\langle x \rangle / t = v$) with a characteristic time scale $\tau$, which increases with viscosity ratio from $M = 30$ (◇) to $M = 100$ (+), 300 (■), 1000 (○), and eventually 10 000 (×), where the crossover has not yet begun.

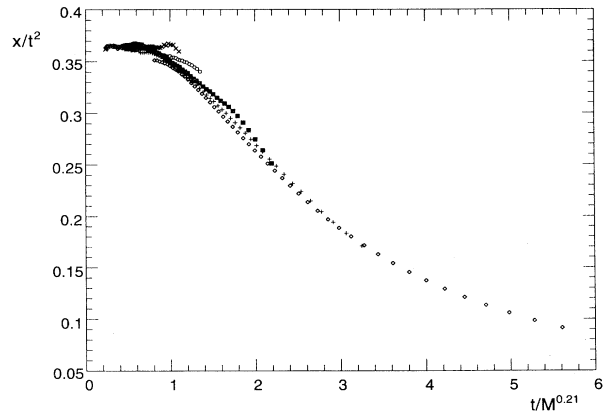


FIG. 6. Plot of $\langle x \rangle / t^2$ vs $t/M^{0.21}$, showing that a characteristic time, which increases with viscosity ratio as $\tau \propto M^{0.21}$, collapses the large-time data, with small deviations approximately $\Delta t \approx 1$ around $t \approx 2$. $M = 30$ (◇), 100 (+), 300 (■), 1000 (○), and 10 000 (×).

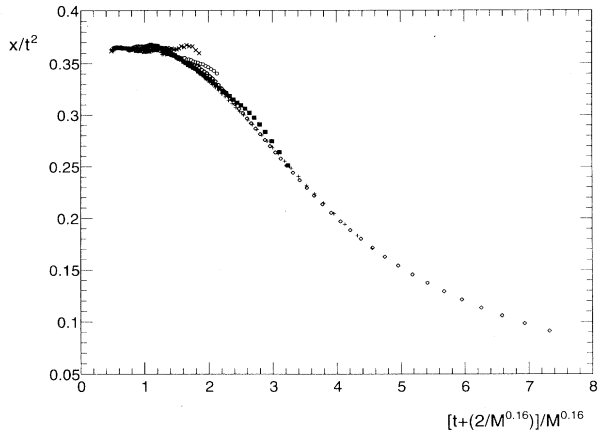


FIG. 7. "Scaling" plot of $\langle x\rangle/t^2$ vs $\{t+2/M^{0.16}\}/M^{0.16}$, showing that an $M$-dependent shift $\Delta \approx 2/M^{0.16}$ accommodates the $t \approx 2$ deviations observed in Fig. 6 with only a small change in the power of the characteristic time, now $\tau \propto M^{0.16}$. $M = 30$, ($\diamond$), 100 (+), 300 (■), 1000 ($\circ$), and 10 000 ($\times$).

the relaxation time changed little from the value in Fig. 6, i.e., from 0.21 to 0.16. In estimating the reliability of this index, we found that, including the shift,the value 0.21 is now too large and that 0.11 is too small; thus we estimate $\tau \approx \tau_0 M^p$, $p = 0.16 \pm 0.05$. Not surprisingly, there is much less certainty in the exponent associated with the small shift, in that $M^{0.5}$ is too strong a dependence and $M^{0.01}$ is too weak a dependence. The essential point to retain from this discussion is that the "scaling" variable provides a good empirical collapse of the data for viscosity ratios occurring in real reservoirs, for $M = 30$ to 1000, with a value of the relaxation time index $p = 0.16 \pm 0.05$, so that

$$\langle x\rangle/t^2 = f(u) \ , \qquad u = \{t + (2/M^{0.16})\}/M^{0.16} \ , \tag{4}$$

where $f(u)$ is the function shown in Fig. 7. The value of the shift exponent and the actual form of the shift have no effect on later results, only serving to improve the data collapse. It seems likely that other forms for the shift could also provide a convincing data collapse, but since the shift must be relatively small, given the data, it is impossible that a different shift could effect a significant change in $p$ since that dependence is dominated by long-time behavior.

## IV. DISCUSSION

It should not be surprising that the apparent accuracy of our results in three dimensions is less than we found in 2D. The most important cause of this loss of precision is the restriction to shorter times. This restriction to shorter times occurs for three reasons: (i) breakthrough occurs sooner for 3D fractals, where the flow advances as $x \approx t^2$, than it did in 2D, which fractal flow advanced more slowly as $x \approx t^{1.4}$; (ii) the crossover is occurring for larger viscosity ratios, which break through earlier than the smaller viscosity ratios studied in 2D; (iii) in 3D our largest systems ($50 \times 50 \times 50$) have 125 000 pore bodies, but they are only 50 pore bodies long, so that breakthrough occurs earlier than it did in 2D,where our largest systems were 96 pore bodies long by 640 wide, containing only 61 440 pore bodies. Therefore, not only does the inevitable greater increase in the number of pore bodies with linear size in 3D restrict us to smaller systems, but also the flows advance faster in 3D than they did in 2D, so that we are restricted to even shorter times than the usual geometrical factors would indicate.

Even so, there is good quantitative evidence for a small power-law dependence of the crossover time on viscosity ratio. It is surprising that the power law is negligibly different in 3D from what it was in 2D. Whether this indicates that the fractal-to-compact relaxation is fundamentally insensitive to dimensionality or the small power law is mimicking some sort of logarithmic singularity is not clear. In any case, the crossover expressions in Eq. (4) convincingly represent the viscosity-ratio dependence of the interfacial position for a reasonable range of viscosity ratios.

The dependence of front velocity on viscosity ratio can now be determined in a straightforward manner. Since all flows become compact for finite viscosity ratio in the limit of large times, $\langle x\rangle/t \to v(M)$, obviously, $\langle x\rangle/t^{1+\varepsilon} \to v(M)t^{-\varepsilon}$; with Eq. (4) this implies that $f(u) \to v_0 u^{-\varepsilon}$, since $u \to t/M^p$. As we see empirically from Fig. 7, all the viscosity-ratio dependence is in $u$, not in the functional form of $f$. Therefore,

$$\langle x\rangle/t^{1+\varepsilon} = f(u) \to v_0 u^{-\varepsilon} = v_0 (M^p/t)^{\varepsilon} \ , \tag{5}$$

so that

$$v(M) = v_0 M^{p\varepsilon} \ ,$$

where $p\varepsilon = 0.16 \pm 0.08$, given the value $\varepsilon = 1.0 \pm 0.2$ and our determination of the relaxation time exponent $p$.

Extending the "fractal" scaling of Ref. [19] to finite viscosity ratio in 3D shows that the factor $v(M)$ occurs in the fractal flow curves as a Koval-type factor [35] for long times (after the flow has become compact). In this long-time limit, we can ignore the time shift $\Delta$, so that the finite viscosity crossover variable becomes $u \to t/M^p$. The logical form for the saturation that obeys both the "scaling" forms is

$$S(x,t,M) = t^{-\varepsilon} s(x/t^{1+\varepsilon}, t/M^p) \ . \tag{6}$$

One can show that this is the general form that satisfies Eq. (4) [19]. Since the flow becomes compact at long enough times, $t \gg \tau$ (i.e., large $u = t/M^p$),

$$S(x,t,M) \to A\zeta\left(b\frac{x}{t}\right) \ . \tag{7}$$

Therefore for large $u$, when the flow is compact,

$$t^{-\epsilon}s(w = x/t^{1+\epsilon}, u = t/M^p) \to A\zeta\left(b\frac{x}{t}\right) . \quad (8)$$

The only way that Eq. (8) can be satisfied (i.e., the only way that the right-hand side of Eq. (8) can be written in terms of the "scaling" variables $u$ and $w$) is for the factors of $t^\epsilon$ on the left-hand side to be canceled by factors of $u^{-\epsilon}$. That is,

$$t^{-\epsilon}s(w = x/t^{1+\epsilon}, u = t/M^p) \to (t^{-\epsilon})(u^\epsilon)\zeta\left(\frac{x}{t^{1+\epsilon}}u^\epsilon\right)$$

$$= M^{-p\epsilon}\zeta\left(\frac{x}{M^{p\epsilon}t}\right) . \quad (9)$$

Therefore, the saturation is decreased by the factor $M^{p\epsilon}$, so that in the fractional flow $F_I$, the saturation $S$ must be increased by the factor $M^{p\epsilon}$. Hence, the $x/t^{1+\epsilon}$ in $F_I = F(x/t^{1+\epsilon})$ is replaced by $M^{p\epsilon}S$, giving

$$F_I = F(M^{p\epsilon}S) . \quad (10)$$

This supports our conjecture that the fractal-to-compact crossover provides a fundamental understanding of the empirical Koval expression for the dependence of fractional flow on saturation and viscosity ratio in the linear-flow regime.

## ACKNOWLEDGMENTS

M.F. gratefully acknowledges the support of the Fossil Energy Program, U.S. Department of Energy, partly through the ORISE Program administered by Oak Ridge Associated Universities, during the early stages of this work. J.C.G. would like to thank the Goldwater Program for financial support.

[1] G. Daccord, J. Nittmann, and H. E. Stanley, in *On Growth and Form*, edited by H. E. Stanley and Ostrowsky (Nijhoff, Dordrecht, 1986).
[2] J. Feder, *Fractals* (Plenum, New York, 1988).
[3] T. Vicsek, *Fractal Growth Phenomena* (World Scientific, Singapore, 1989).
[4] R. Lenormand, E. Touboul, and C. Zarcone, J. Fluid Mech. **189**, 165 (1988).
[5] V. Frette, J. Feder, T. Jossang, P. Meakin, and K. J. Maloy, Phys. Rev. E **50**, 2881 (1984).
[6] M. Ciepla and M. O. Robbins, Phys. Rev. B **41**, 11 508 (1990).
[7] K. J. Maloy, A. Hansen, E. L. Hinrichsen, and S. Roux, Phys. Rev. Lett. **213**, (1992).
[8] M. Matushita, in *The Fractal Approach to Heterogeneous Chemistry*, edited by X. Avnir (Wiley, New York, 1989).
[9] R. M. Brady and R. C. Ball, Nature (London) **309**, 225 (1984).
[10] D. Barkey, J. Electrochem. Soc. **138**, 2912 (1992).
[11] P. Meakin, J. Feder, and T. Jøssang, Physica A **176**, 409 (1991).
[12] H. Inaoka, and H. Takayasu, Phys. Rev. E **47**, 899 (1993).
[13] L. Niemeyer, L. Pietronero, and H. Wiesman, Phys. Rev. Lett. **52**, 1033 (1984).
[14] B. Grier, E. Ben-Jacob, R. Clarke, and L. M. Sander, Phys. Rev. Lett. **56**, 1264 (1986).
[15] P. Carro, S. L. Marchiano, A. Hernandez-Creus, S. Gonzales, C. Salvarezza, and A. J. Arvia, Phys. Rev. E **48**, R2374 (1993).
[16] M. Ferer, R. A. Geisbrecht, W. N. Sams, and D. H. Smith, Phys. Rev. A **45**, 6973 (1992).
[17] M. Ferer, W. N. Sams, R. Geisbrecht, and D. H. Smith, Phys. Rev. E **47**, 2713 (1993).
[18] M. Ferer and D. H. Smith, Phys. Rev. E **49**, 4114 (1994).
[19] M. Ferer, W. N. Sams, R. A. Geisbrecht, and D. H. Smith, AlChE J. **49**, 749 (1995).
[20] R. E. Collins, *Flow of Fluids Through Porous Materials* (Reinhold, New York, 1961).
[21] H.-K. Rhee, R. Aris, and N. R. Amundson, *First-Order Partial Differential Equations: Vol. 1, Theory and Applications of Single Equations* (Prentice-Hall, Englewood Cliffs, NJ, 1986).
[22] P. Meakin, Phys. Rev. A **27**, 604 (1983).
[23] P. Meakin, *The Fractal Approach to Heterogeneous Chemistry* (Ref. [8]).
[24] B. B. Mandelbrot, *The Fractal Geometry of Nature* (Freeman, New York, 1992).
[25] P. G. Saffman and G. I. Taylor, Proc. R. Soc. London A **245**, 312 (1958).
[26] K. J. Maloy, J. Feder, and T. Jossang, Phys. Rev. Lett. **55**, 2688 (1985).
[27] P. Meakin, Phys. Rev. A **27**, 2616 (1983).
[28] J. Nittmann, G. Daccord, and H. E. Stanley, Nature (London) **314**, 141 (1985).
[29] J.-D. Chen and D. Wilkinson, Phys. Rev. Lett. **55**, 1892 (1985).
[30] H. Siddiqui and M. Sahimi, Chem. Eng. Sci. **45**, 163 (1990).
[31] P. R. King, J. Phys. A **20**, L529 (1987).
[32] I. Fatt, Trans. Am. Inst. Mech. Eng. **207**, 144 (1956).
[33] D. W. Peaceman, *Fundamentals of Numerical Reservoir Simulation* (Developments in Petroleum Science) (Elsevier, Amsterdam, 1977).
[34] G. W. Thomas, *Principles of Hydrocarbon Reservoir Simulation* (International Human Resources Development, Boston, 1982).
[35] E. J. Koval, Soc. Pet. Eng. AIME Pap. **228**, 145 (1963).

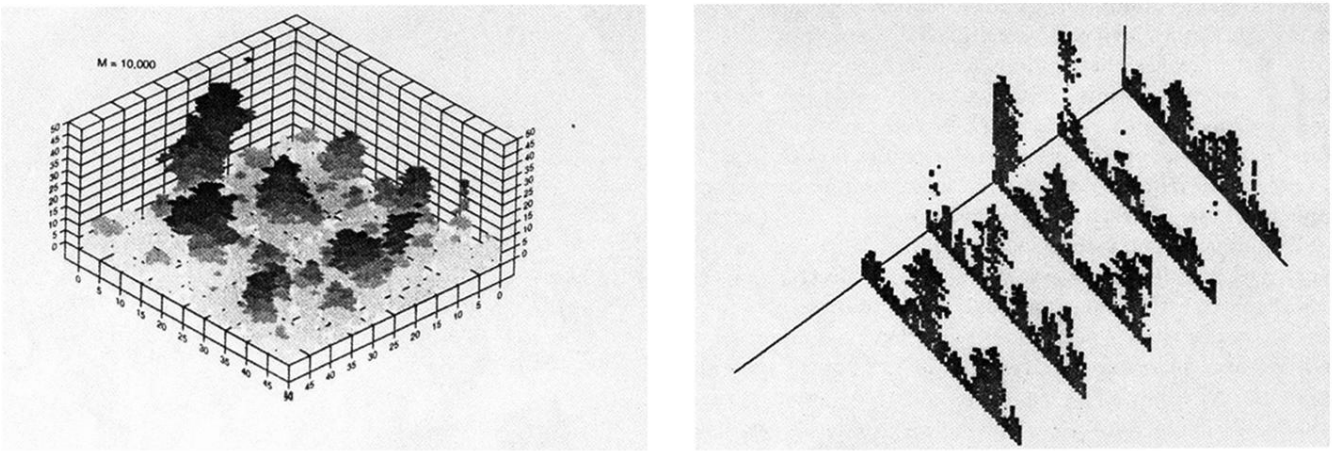


FIG. 1. Near-breakthrough flow pattern showing the pore bodies and throats occupied by injected fluid for a $50 \times 50 \times 50$ porous medium resulting from our simulations with a fluid velocity ratio $M = 10\,000$. For clarity, we present both a shaded 3D plot (on the left), in which the gray scale darkens with height, and projections of slices (on the right). The periodic boundary conditions are obvious in that fingers on one side continue on the other (notably, in the middle slice; also there is a connection between fingers ending in the last slice and starting in the first). The characteristics of DLA patterns are present: many short fingers coarsening to fewer and fewer longer fingers.

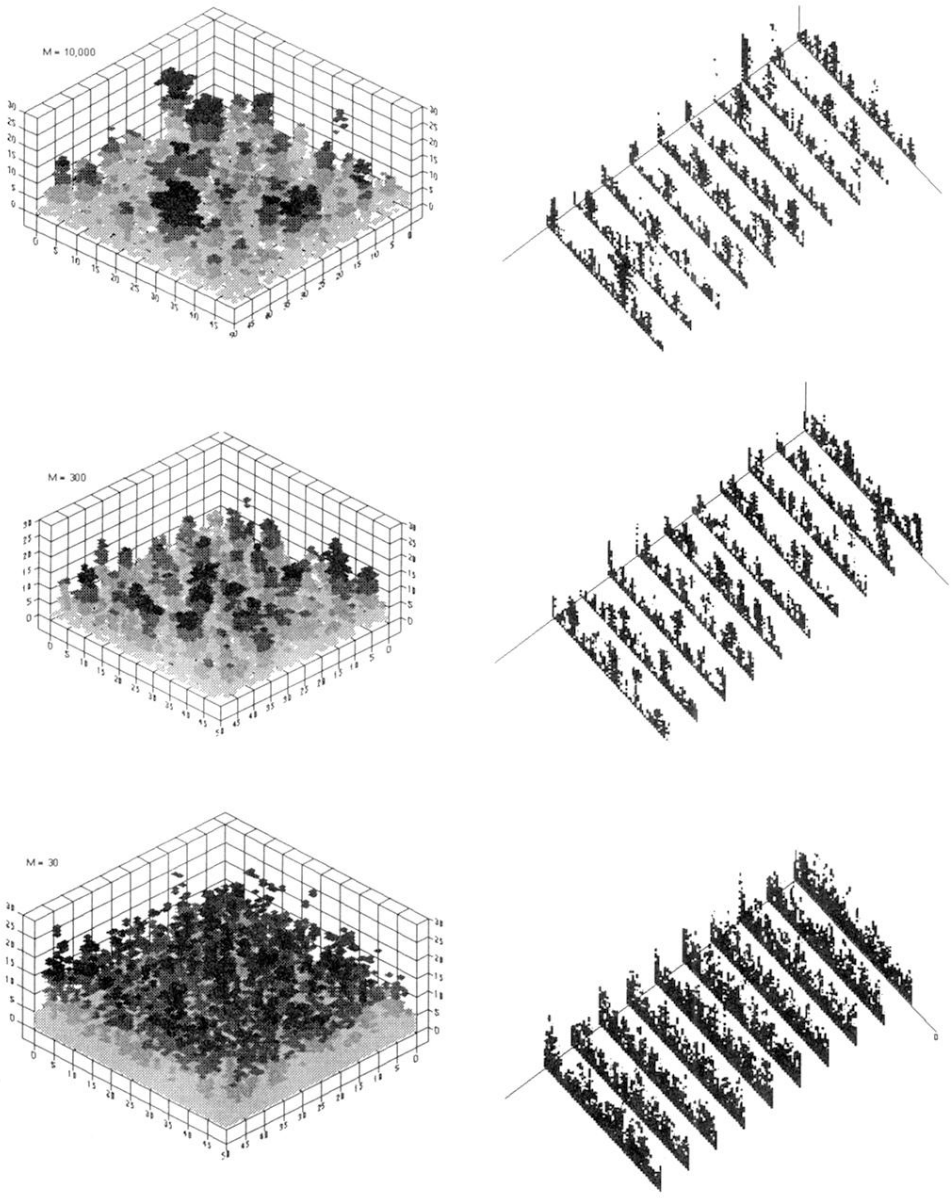


FIG. 3. Near-breakthrough flow patterns (both shaded 3D and projections of slices) show the locations of pore bodies occupied by injected fluid for three different viscosity ratios, $M = 10\,000$, 300, and 30. Note the apparent crossover from the fractal, DLA-like pattern at $M = 10\,000$ to compact flow with a rough interface at $M = 30$. Because of fluctuations in the pressure gradient perpendicular to the primary flow direction, we find the same fragmentation of the interface for $M = 30$, observed in 2D for linear flow with the smaller viscosity ratios.